Covariation of axon initial segment location and dendritic tree normalizes the somatic action potential

Mustafa S. Hamada[a,b], Sarah Goethals[c], Sharon I. de Vries[a], Romain Brette[c], and Maarten H. P. Kole[a,b,1]

[a]Department of Axonal Signaling, Netherlands Institute for Neuroscience, Royal Netherlands Academy of Arts and Sciences (KNAW), 1105 BA Amsterdam, The Netherlands; [b]Cell Biology, Faculty of Science, Utrecht University, 3584 CH Utrecht, The Netherlands; and [c]Sorbonne Universités, Université Pierre et Marie Curie (UPMC) Univ Paris 06, INSERM, CNRS, Institut de la Vision, 75012 Paris, France

Edited by Bruce P. Bean, Harvard Medical School, Boston, MA, and approved November 4, 2016 (received for review May 12, 2016)

In mammalian neurons, the axon initial segment (AIS) electrically connects the somatodendritic compartment with the axon and converts the incoming synaptic voltage changes into a temporally precise action potential (AP) output code. Although axons often emanate directly from the soma, they may also originate more distally from a dendrite, the implications of which are not well-understood. Here, we show that one-third of the thick-tufted layer 5 pyramidal neurons have an axon originating from a dendrite and are characterized by a reduced dendritic complexity and thinner main apical dendrite. Unexpectedly, the rising phase of somatic APs is electrically indistinguishable between neurons with a somatic or a dendritic axon origin. Cable analysis of the neurons indicated that the axonal axial current is inversely proportional to the AIS distance, denoting the path length between the soma and the start of the AIS, and to produce invariant somatic APs, it must scale with the local somatodendritic capacitance. In agreement, AIS distance inversely correlates with the apical dendrite diameter, and model simulations confirmed that the covariation suffices to normalize the somatic AP waveform. Therefore, in pyramidal neurons, the AIS location is finely tuned with the somatodendritic capacitive load, serving as a homeostatic regulation of the somatic AP in the face of diverse neuronal morphologies.

axon initial segment | action potential | dendrites | axon | computational model

The axon initial segment (AIS) specifies in vertebrate neurons a single domain for the final integration of synaptic input and the initiation of action potentials (APs) (1, 2). To rapidly produce large inward and outward currents mediating the AP, the AIS contains a complex arrangement of cytoskeletal and transmembrane proteins clustering high densities of voltage-gated sodium (Nav) and potassium (Kv) channels in the axolemma (2–4). Although the composition of ion channels is critical for initiation and regulation of firing patterns, there are emerging insights that the AIS is not operating in isolation but is also subject to activity-dependent changes in size and location constrained by the local dendritic branch geometry and the passive cable properties (5–7). Experimental studies linking changes in AIS length and neuronal output showed that an increased length facilitates AP generation (6, 8). In these cases, the net increased excitability is a logical consequence of the larger Nav conductance. However, predicting the impact of AIS location on neuronal output is more complex. Experimental studies showed that an activity-dependent distal shift of the AIS is associated with decreased AP output (5). In contrast, model simulations showed that shifting the AIS distally promotes excitability (9). One of the critical factors influencing AIS excitability is the large somatodendritic membrane area acting as current sink for sodium current generated in the AIS (10–12). In this view, a distal anatomical location of the AIS increases electrical compartmentalization and facilitates axonal AP generation. Indeed, the local depolarization in the AIS is proportional to the axial resistance between the soma and the AP initiation site, which increases with distance from the soma (11). However, increasing the distance between soma and AIS will be unfavorable for synapse to spike coupling, because it increases voltage attenuation and thereby, reduces the possibility for synaptic potentials to cross the AP threshold in the AIS (13). Furthermore, pyramidal neurons require axonal APs to rapidly depolarize the soma and activate somatic voltage-gated Nav channels to produce the dendritic back-propagating AP (14, 15).

In view of the importance of AIS location in neuronal excitability, it is striking that the reported intercellular variability within neuron cell types is large. In 50 to 70% of dopaminergic and GABAergic neurons of the substantia nigra, the axon arises from dendrites, even up to ∼260-μm distance from the soma (16–18). In fact, an axon origin from a dendrite is even a defining feature of some hippocampal interneurons (19, 20). Furthermore, about 30 to 60% of the pyramidal neurons in the hippocampus have an axon emerging from a basal (or sometimes, an apical) dendrite up to ∼40-μm distance from the soma (20, 21), and also, in the neocortex, axons have been observed to emerge from basal dendrites (19, 22, 23). Here, we investigated whether AIS location plays a functional role in neocortical pyramidal neuron excitability. We found that AIS distance from the soma but not length strongly and inversely correlates with the dendritic morphology and follows the theoretical relationship predicted by cable theory when resistive coupling between the soma and axon adjusts a longitudinal current that normalizes somatic AP generation. The large intercellular variation in AIS location thus reflects structural homeostatic scaling to normalize the somatic AP in the face of diverse morphologies of dendritic trees.

Significance

Neurons generate highly reliable and temporally precise action potentials with a spatial onset in the axon initial segment. The axon initial segment location relative to the soma is, however, highly variable across neurons within the same cell class. Here, we experimentally and theoretically investigated the structure–function relationship of axon distances in neocortical pyramidal neurons. We discovered a scaling principle between the size of the dendritic tree and the axon distance supported by the cable properties and electrophysiological recordings. The work reveals that axons are not randomly positioned but covary with dendrites normalizing the somatic action potential in the face of diverse cellular morphologies.

Author contributions: M.H.P.K. designed research; M.S.H., S.G., S.I.d.V., R.B., and M.H.P.K. performed research; R.B. contributed new reagents/analytic tools; M.S.H., S.G., R.B., and M.H.P.K. analyzed data; and M.S.H., R.B., and M.H.P.K. wrote the paper.

The authors declare no conflict of interest.

This article is a PNAS Direct Submission.

Freely available online through the PNAS open access option.

[1]To whom correspondence should be addressed. Email: m.kole@nin.knaw.nl.

This article contains supporting information online at www.pnas.org/lookup/suppl/doi:10.1073/pnas.1607548113/-/DCSupplemental.

Results

Thick-Tufted Layer 5 Neurons Have Diverse Axonal Origins. To characterize the diversity in axon locations in layer 5 pyramidal neurons, we colabeled tissue sections containing the primary somatosensory hind limb region from adult Wistar rats with Gp-anti–NeuN, a somatodendritic marker, Rb–anti-Ankyrin G, an AIS marker, and M-anti–SMI-32 (Sternberger monoclonal-incorporated antibody 32), a neurofilament marker, for type 1 (thick-tufted) layer 5 neurons (24) (Fig. 1*A*). SMI-32$^+$ primary axons could be observed emanating from either the soma or a basal dendritic branch (Fig. 1*B*). Population analysis (n = 7 animals; two to three sections per animal) showed that neurons with an axon origin from a dendrite, hereby referred to as "axodendritic" neurons, constitute one-third of the population of SMI-32$^+$ neurons (Fig. 1*C*). The large fraction of pyramidal neurons with an axon starting from a basal dendrite may indicate that they represent a distinct subtype. Based on electrophysiological and anatomical features, two major types of layer 5 pyramidal neurons have been identified: intracortically (corticocortical) projecting slender tufted layer 5 neurons and subcortically [corticosubcortical (CS)] projecting thick-tufted layer 5 neurons (24–26). Although SMI-32 typically labels thick-tufted layer 5 neurons, they may be further divided into subpopulations (24, 25). To test whether axodendritic and axosomatic neurons project to different targets, we injected fluorescent retrograde beads in the spinal cord (C2/3) (Fig. S1). Fluorescent retrobeads were localized exclusively in the somata of superficial and deep layer 5 neurons in the somatosensory and motor cortices. From a total of 313 analyzed neurons, 178 were back-labeled with fluorescent retrobeads. Within the population of layer 5 neurons with identified axon origin (somatic or dendritic), 58% of the axosomatic neurons projected to C2/3 (n = 160 of 277) compared with 46% of the axodendritic neurons (n = 17 of 37; Fisher's exact test, P = 0.2167) (Fig. S1), indicating equal subcerebral targeting of both subtypes. Next, we made whole-cell recordings from visually identified pyramidal layer 5 neurons and filled them with biocytin for posthoc immunofluorescence using βIV-spectrin to identify the axon location (n = 38 cells; 27 animals). Similarly, a large fraction of neurons was axodendritic (50%; n = 19 of 38). The dendritic organization of both subtypes showed that apical dendrites branched extensively in layer 1, consistent with a CS cell type (Fig. 1*D*, Fig. S2, and Table S1). Interestingly, quantitative analysis showed that the sum of dendritic branches was smaller in the basal region of the axodendritic neurons (Fig. 1*E* and Table S1). This difference was further supported by a Sholl analysis revealing that the density of basal dendrites was significantly lower in axodendritic neurons (two-way ANOVA, $P < 0.05$, n = 26) (Fig. 1*F*). Additional comparison of branches as a function of distance from the soma showed that axodendritic neurons have fewer (basal and apical) dendritic sections within a proximal region of 100–200 μm from the cell body and a lower complexity of both basal and apical dendritic sections (Fig. 1 *F* and *G*). Taken together, these results indicate that the subcellular axon origin is not associated with a specific subtype but is associated with quantitative differences in the dendritic tree.

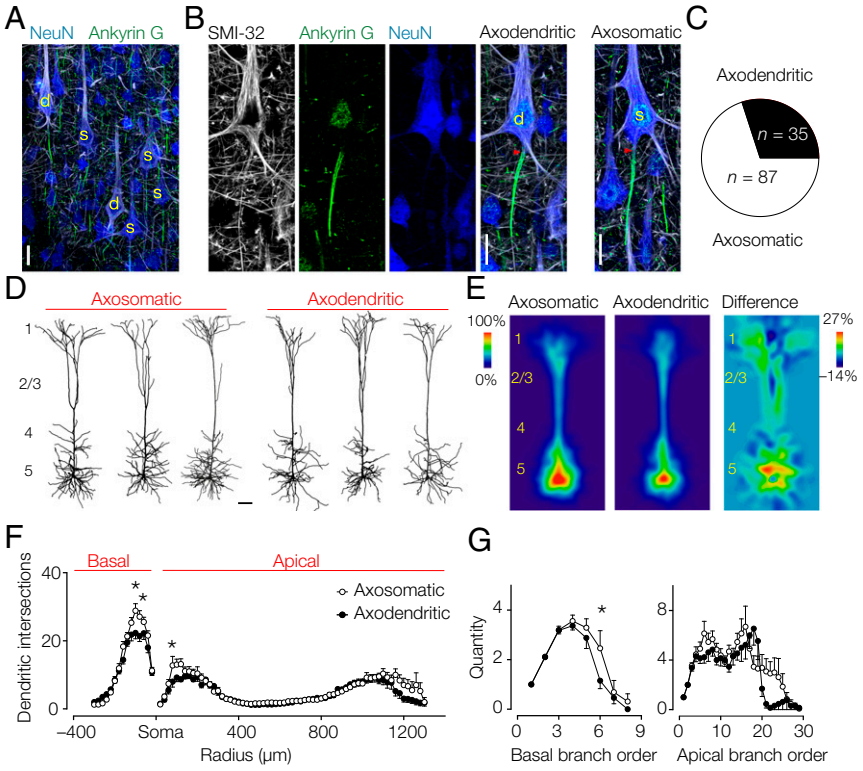

Fig. 1. Axodendritic layer 5 pyramidal neurons are abundant in the neocortex and characterized by a smaller dendritic tree. (*A*) *z*-Projected confocal scan of a triple-immunofluorescence labeling for NeuN (somatodendritic marker; blue), Ankyrin G (an AIS marker; green), and SMI-32 (type 1 pyramidal cell marker; white). SMI-32$^+$ neurons with identified axon location are indicated (yellow). (Scale bar: 25 μm.) (*B*, *Left*) Single fluorescence channels and merged image of an axodendritic neuron. (*B*, *Right*) Merged scan of an axosomatic neuron. Red arrowheads indicate the start of the AIS. d, Axodendritic; s, axosomatic. (Scale bar: 20 μm.) (*C*) Axodendritic neurons constitute one-third of the SMI-32$^+$ neurons (28.7%; 35 of 122). (*D*) Representative examples of 3D reconstructed dendritic trees of axosomatic and axodendritic neurons. (Scale bar: 100 μm.) (*E*) Average heat maps of (*Left*) axosomatic (n = 13) and (*Center*) axodendritic (n = 13) neurons. (*Right*) Note the higher density of basal dendrites in the subtracted heat map. (*F*) Sholl plot of axosomatic (○) and axodendritic (●) neurons at 20-μm intervals. Two-way repeated measures ANOVA interaction P = 0.0651, intersections $P < 0.0001$, and subtype $P < 0.0001$. Bonferroni's posthoc test. Error bars represent SEM. *$P < 0.05$. (*G*) Axodendritic neurons possess lower branch order of the basal dendrites. Basal branch order: two-way ANOVA interaction P = 0.3468, branch order $P < 0.0001$, and subtype P = 0.030. Bonferroni's posthoc test. Apical branch order: two-way ANOVA interaction P = 0.0165, branch order $P < 0.0001$, and subtype P = 0.0016. Error bars represent SEM. *$P < 0.05$.

The Dendritic Morphology Scales Specifically with AIS Distance. Salient characteristics of axodendritic layer 5 neurons were their relatively narrow diameter of the proximal apical dendritic trunk (Fig. 2 *A* and *B* and Table S2) and smaller somatic cross-sectional area (Fig. 2 *A* and *B* and Table S2), consistent with their reduced dendritic organization (Fig. 1 *E* and *F*). To obtain a single measure for AIS location, we determined the AIS distance (AISΔ) as the linear path length from the base of the soma to the start of the dense expression of either βIV-spectrin or Ankyrin G (Fig. 2*A*). In contrast to previous observations in mouse hippocampal pyramidal neurons (21), we never detected Ankyrin G or βIV-spectrin immunofluorescence signals in the dendritic branches connecting the axon, suggesting that AISΔ accurately reflects the anatomical distance from the soma. In axodendritic neurons, AISΔ was significantly more distal compared with axosomatic neurons (Fig. 2 *A* and *B* and Table S2). The size of the AIS compartment was, however, constant; neither AIS length nor the 2D area were different between subtypes (Table S2). Interestingly, specifically, the AISΔ inversely and strongly correlated with the apical dendrite diameter (Fig. 2*C* and Table S3). A correlation between the axonal and dendritic organization was further corroborated when plotting AISΔ against the total number of dendritic nodes (Fig. 2*D* and Table S3) and the total dendritic length as well as the total dendritic area (Fig. S3). In contrast, neither AIS length nor the area correlated with apical dendritic diameter (Table S3). These findings suggest that, in the population of thick-tufted layer 5 neurons, the AISΔ is fine-tuned with the anatomical organization of dendrites.

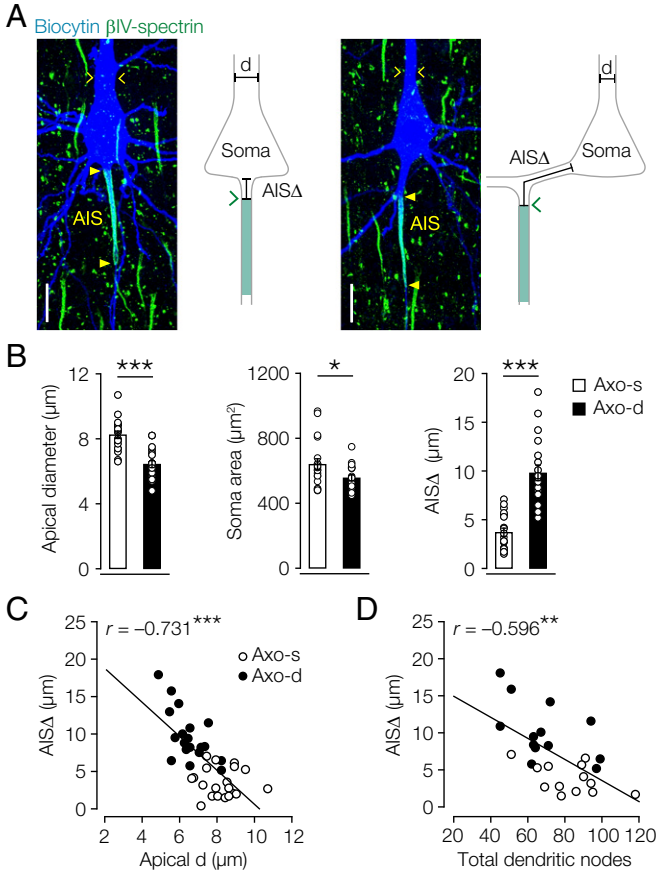

Fig. 2. Dendritic morphology correlates with AIS distance. (*A*, *Left*) *z*-Projected confocal images of filled axosomatic and axodendritic layer 5 neurons (blue) overlaid with βIV-spectrin (green). (*A*, *Right*) Schematic with AISΔ indicating the linear path from soma base to start of βIV-spectrin expression. Yellow closed arrowheads indicate start and end of the βIV-spectrin immunofluorescence signal; yellow open arrows indicate apical dendrite diameter. *d*, Apical diameter. (Scale bar: 20 μm.) (*B*) Axodendritic neurons possess smaller apical dendritic diameter and somata but longer AISΔ. Two-way unpaired student's *t* test. Axodendritic, $n = 19$; axosomatic, $n = 19$. Error bars represent SEM. Axo-d, axodendritic; Axo-s, axosomatic. $^{*}P < 0.05$; $^{***}P < 0.00001$. (*C*) Correlation analysis between AISΔ and apical dendrite diameter. Pearson's test; $n = 38$. $^{***}P < 0.0001$. (*D*) Correlation analysis between AISΔ and total sum of dendritic nodes. Pearson's test; $n = 26$. $^{**}P = 0.001$.

Somatodendritic Capacitive Load Predicts Axonal Coupling Resistance. To examine whether AISΔ, ranging from 1.5 to 20 μm, impacts neuronal excitability, we examined the somatically recorded AP properties. The first rate of rise ($dV_m\ dt^{-1}$) component of the somatic AP reflects the axonal axial current charging the somatodendritic capacitor (14). If the local somatodendritic capacitance is constant, $dV_m\ dt^{-1}$ is expected to vary as a function of AISΔ because of the axial resistance (R_a). In striking contrast to the predictions, the first peak in the $dV_m\ dt^{-1}$ showed no difference between the subtypes (Fig. 3 *A*–*C*, Fig. S4, and Table S4), and did not correlate with AISΔ (Fig. 3*C*). Similarly, the second, somatic component was also not different (Table S4). Also, the onset rapidness, defined as the slope of a linear fit to the AP phase plot ($dV_m\ dt^{-1}$ vs. V_m; with units of milliseconds^{-1}), was not different (~78 ms^{-1}) (Table S4). Theoretical work predicts that increasing AISΔ is associated with a more hyperpolarized AP voltage threshold (11). Although AP voltage threshold was significantly more hyperpolarized in axodendritic neurons (~3 mV, $P = 0.0005$) (Table S4), it did not correlate with AISΔ ($r = –0.332$, $P = 0.055$) (Table S3). The AP voltage threshold rather correlated with the apical dendritic diameter ($r = 0.488$, $P = 0.003$) (Table S3), and the larger apical dendritic diameter (capacitive load) required larger current amplitudes to reach threshold compared with axodendritic neurons ($P = 0.0095$) (Table S4). Taken together, AISΔ alone does not explain differences in spike generation.

If the maximal Nav conductance ($\bar{g}_{Na}$) within the AIS is constant, the axial current should theoretically be larger with a more proximal AIS location. Because the somatodendritic capacitance (C_m) acts as a current sink, the axial current I_{axon} should flow toward the soma and leave the neuron as capacitive current: $I_{axon} = C_m \times dV_m\ dt^{-1}$. Based on these concepts, we hypothesized that the larger capacitance of axosomatic neurons is matched with the larger axial current expected for more proximal AIS locations. This idea is supported by the observation that apical dendrites in the axosomatic neurons are, on average, ~2 μm larger in diameter (Fig. 2 *A* and *B*) and strongly correlated with the AISΔ (Fig. 2*C* and Table S3). It may be predicted that AISΔ is inversely proportional to the capacitance of a characteristic length of apical dendrite, which scales as $d^{-3/2}$, where d is the apical dendritic diameter. Indeed, correlation of the transformed geometrical data showed that AISΔ is well-predicted by apical $d^{-3/2}$ (Fig. 3*D*). To examine more closely the relationship with resistive coupling (R_a), we determined for each cell the specific coupling R_a based on the 3D reconstructions assuming a specific intracellular cytoplasmic resistance (R_i) of 150 Ω cm (*Materials and Methods*). Interestingly, there was a strong linear relationship between R_a and AISΔ (Fig. 3*E*), suggesting that branch diameters are not greatly different between the subtypes. Next, using the coupling R_a estimates, we tested whether apical $d^{-3/2}$ is a predictor for R_a and found a significant linear relationship (Fig. 3*F*). These data suggest that resistive coupling increases with smaller dendritic capacitance to reduce I_{axon} during spike initiation and that the scaling of coupling R_a with dendrites is independent of a somatic or dendritic origin of the axon.

Biophysical Analysis of Dendritic and Axonal Tuning of the Somatic AP. To understand how AISΔ influences the capacitive depolarization of the somatodendritic membrane by the axonal AP, we examined a simple biophysical model consisting of a cylindrical axon (diameter of 1.5 μm) connected to a larger cylindrical somatodendritic compartment (diameter of 6 μm and length of

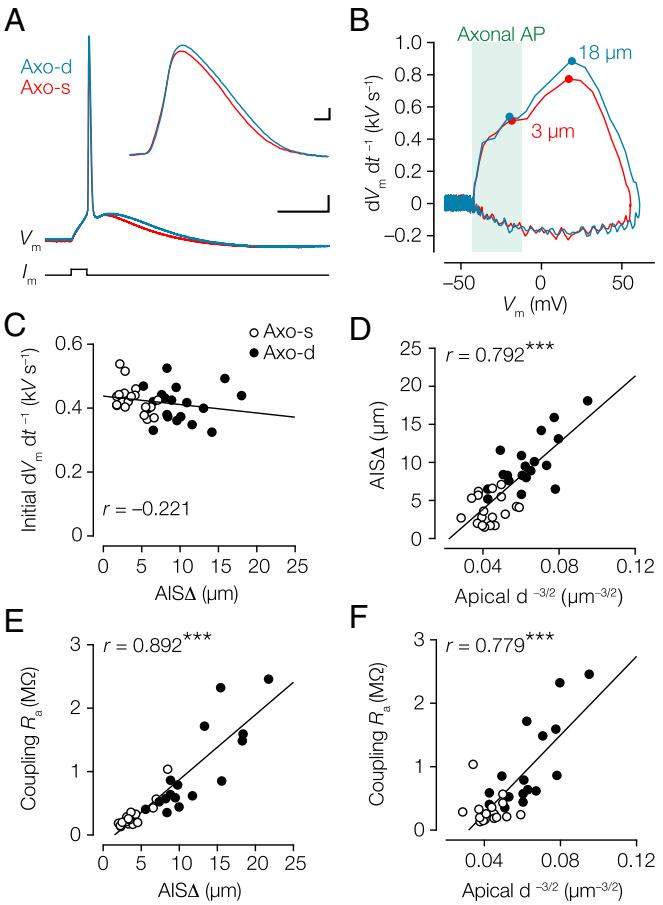

Fig. 3. Similarity in AP waveform but inverted correlation between AIS distance and dendritic diameter. (*A*) Overlaid voltage traces of somatic APs (blue, axodendritic; AISΔ = 18 µm; red, axosomatic; AISΔ = 3 µm). (Scale bar: 10 ms, 10 mV.) (*Inset*) Somatic APs plotted on an expanded timescale. (Scale bar: 0.1 ms, 10 mV.) (*B*) Corresponding phase plots of the APs shown in *A*. (*C*) The first peak in the $dV_m\ dt^{-1}$ did not correlate with AISΔ. Pearson's test ($P = 0.203$); $n = 36$. Axo-d, axodendritic; Axo-s, axosomatic. (*D*) Correlation plot showing AISΔ scales with apical $d^{-3/2}$. Pearson's test; $n = 38$. ***$P < 0.0001$. (*E*) AISΔ distance is linearly related to coupling R_a. Pearson's test; $n = 33$. ***$P < 0.0001$. (*F*) Correlation of apical $d^{-3/2}$ vs. coupling R_a. Pearson's test; $n = 33$. ***$P < 0.0001$.

500 µm) (Fig. 4*A*). Kv channels, somatodendritic Nav conductance, and the inactivation component of Nav channels were excluded (11). When Nav channels open, the membrane potential in the AIS rises toward the sodium reversal potential (E_{Na}) (Fig. 4*B*). Because there were no Nav channels between soma and AIS in the model, this region should be mostly resistive (resistance R_a). Therefore, the axonal current should be $I_{axon} = (E_{Na} - V_s)/R_a$, where V_s is the somatic voltage. We assumed that V_s remains far from E_{Na} and close to spike threshold during the initial rise of the somatic AP owing to the large somatodendritic capacitance (more precisely, V_s rises from spike threshold to somatic threshold, both well below E_{Na}). This simplified account indicated that $I_{axon} \propto 1/R_a$, and because resistance is linearly proportional to the path length (Fig. 3*E*), it follows that $I_{axon} \propto 1/(\text{AIS}\Delta)$. A more precise analysis yields $I_{axon} \propto 1/(\text{AIS}\Delta + \delta)$, where δ is a positive shift calculated from the parameters (Fig. S5 and *SI Materials and Methods*). I_{axon} must charge a large cylindrical somatodendritic compartment with a dendritic diameter (d). The voltage response of a cylinder to a current scales with diameter as $d^{-3/2}$ (27). Therefore, for the voltage response at the soma to be independent of the diameter, AISΔ must scale as $d^{-3/2}$ (*Materials and Methods* and Fig. S5). As predicted, peak I_{axon} and $dV_m\ dt^{-1}$ do not depend on leak currents (Fig. S5) or AIS length in the range tested but are inversely related with AISΔ (Fig. 4*C*). In general, our theoretical analysis predicts that initial $dV_m\ dt^{-1}$ should scale with dendritic diameter as $d^{-3/2}$, and we found numerically and theoretically that those scaling factors were well in line with the experimentally observed relationship (Fig. 4*D*). Finally, is the covariation between dendrites and axons sufficient to tune the somatic AP? To test this idea, we varied the dendritic diameter between 2 and 8 µm in the model and tuned the AISΔ so as to obtain a constant somatic $dV_m\ dt^{-1}$ of 350 V s^{-1}. The results from the numerical simulation (Fig. 4*E*) agreed well with this prediction and showed that the AISΔ and the dendritic size interact as observed experimentally (compare with Fig. 3*D*).

Geometry of the Somatodendritic Compartment Normalizes the Consequence of Axon Coupling to the Dendrite. Next, to test how dendrites and AISΔ interact in neurons with complex morphologies and the presence of voltage-gated channels, we created a

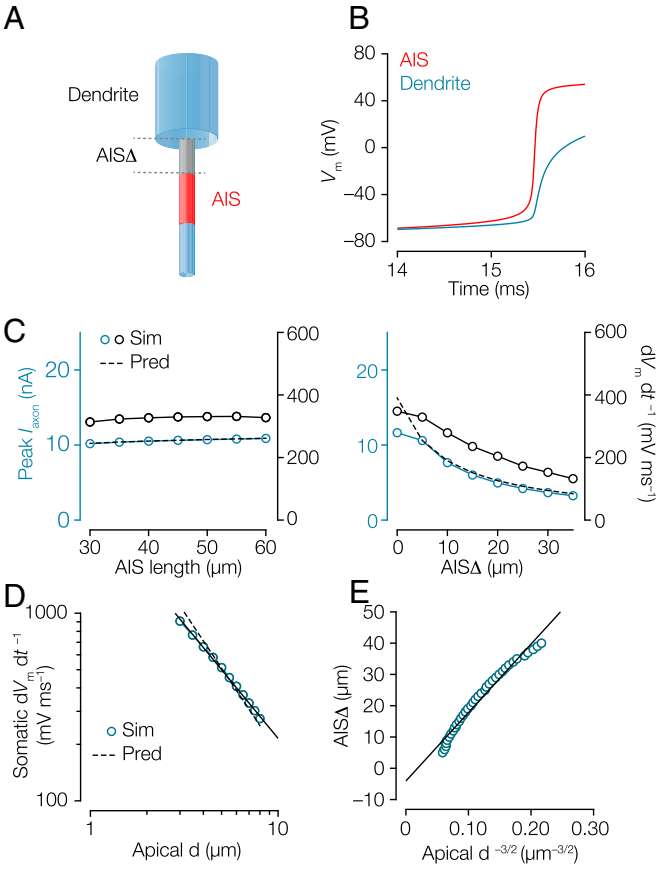

Fig. 4. Numerical simulations predict that dendritic scaling with AIS distance normalizes the somatic AP. (*A*) Illustration of the simplified conductance-based model of a pyramidal neuron with cylindrical dendrite/axon (blue) and AIS (red). AISΔ (gray) is 5-µm and 45-µm long (diameter of 1.5 µm). Nav (m^1) channels do not inactivate, and Kv channels are not included. (*B*) Voltage waveforms of the AIS (red) and soma (blue; interface of axon and dendrite) during AP initiation. Note the lack of repolarization in the simple model. (*C*, *Left*) Somatic I_{axon} and $dV_m\ dt^{-1}$ were independent of AIS length. (*C*, *Right*) Somatic I_{axon} and $dV_m\ dt^{-1}$ showed a strong dependence on AISΔ. (*D*) Somatic $dV_m\ dt^{-1}$ plotted against apical diameter (d) in log–log scale (blue circles). The correlation is fitted with a power law function with exponential of –1.22 (black line) compared with the theoretical prediction of –1.5 (black dashed line). (*E*) Combination of *C*, *Right* and *D*. AISΔ was adjusted to obtain a constant somatic $dV_m\ dt^{-1}$ of 350 V s^{-1} for dendrite diameters between 2.0 and 8.0 µm and plotted as a function of $d^{-3/2}$ (blue circles). The line represents the linear regression of the data.

conductance-based multicompartmental model based on an axosomatic layer 5 pyramidal neuron (*Materials and Methods* and Fig. 5*A*). Based on the βIV-spectrin immunofluorescence signal, the AISΔ (2.1 μm) and AIS length (39.5 μm) were precisely implemented in the model (28) (Fig. S6). To test the role of R_a in the optimized model, we fixed the diameter of the section representing AISΔ to 2 μm and varied the segment length between 2 and 40 μm (Fig. 5 *B* and *C*). The critical role of AISΔ was evident by the steep hyperpolarization of the voltage threshold (Fig. S6) and the decrease of the initial $dV_m\ dt^{-1}$ of the model APs (Fig. 5*C*) in similar magnitude as predicted with the simplified biophysical model (Fig. 4*C*). With an AISΔ of 30 μm, the initial $dV_m\ dt^{-1}$ reduced substantially, causing a temporal delay in the onset of the somatic AP and producing, subsequently, AP reflection in the axon. With an AISΔ of 40 μm, the somatic AP failed (Fig. 5 *B* and *C*). Increasing AISΔ thus facilitates axonal output but negatively impacts the antidromic AP. Finally, to test whether the reduction of I_{axon} with distal AIS positions can be accounted for by reducing the somatodendritic capacitive load, we positioned the AIS at ~18 μm from the soma. The AIS shift reduced the initial rising phase of the somatic AP by ~179 V s^{-1} (Fig. 5*D*), in line with the expected increase in resistive coupling (Fig. 4*C*). Furthermore, in agreement with the numerical and theoretical predictions, when the somatic and apical dendritic diameters were reduced by 30% (reflecting the average dendritic diameter of axodendritic neurons) (Fig. 2*B*), the initial peak in the $dV_m\ dt^{-1}$ increased selectively and reached approximately similar amplitude compared with the control AP (Fig. 5*D*). Together, these simulations with realistic morphologies show that covariation of dendritic geometry and AIS distance suffices to tune the somatic AP.

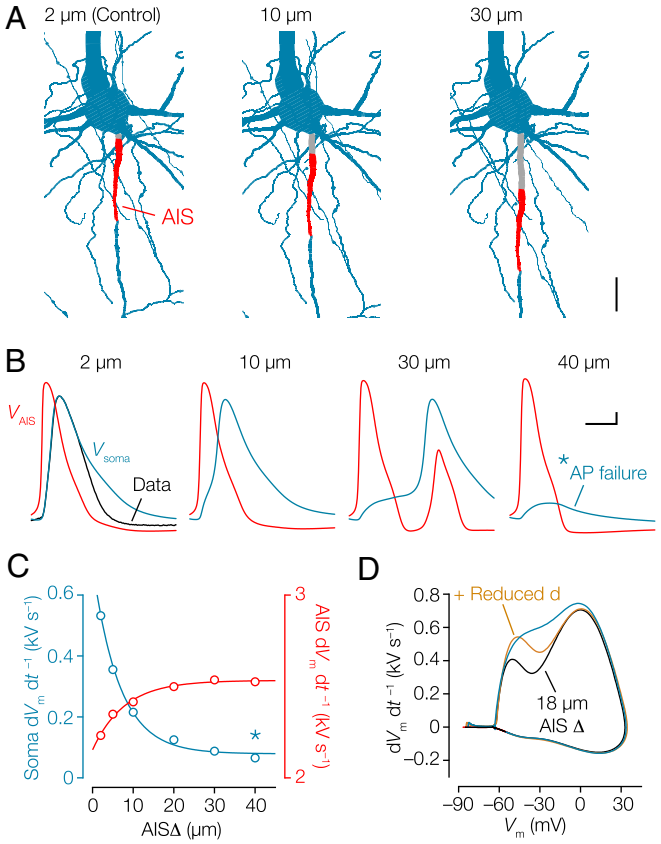

Fig. 5. Dendritic morphology and AIS distance in a realistic compartmental model normalize the somatic AP. (*A*) Part of the morphological reconstruction encompassing soma, proximal basal and apical dendrites (blue), and the AIS (red) used in compartmental modeling. The AISΔ of 2 μm represents the control morphology. Alternative models were made with increasing AISΔ (gray). (Scale bar: 20 μm.) (*B*) Simulation of single APs at the soma (blue) overlaid with the experimentally recorded AP as constraint (black) and corresponding simulated AP waveform in the distal AIS (red). Somatic and AIS APs for different AISΔ values. Note the failure of somatic (but not axonal) AP generation with a 40-μm AISΔ. (Scale bar: 0.1 ms, 10 mV.) (*C*) First $dV_m\ dt^{-1}$ of the somatic APs (blue) and the peak $dV_m\ dt^{-1}$ of the AIS AP (red). Data series are fitted with single exponential functions. *Somatic AP failure. (*D*) Phase plot of the simulated APs showing how adjusting AISΔ to 18 μm reduced the first $dV_m\ dt^{-1}$ by ~179 V s^{-1}. Decreasing the somatodendritic compartment by 30% sufficed to recover the amplitude in the first $dV_m\ dt^{-1}$.

Discussion

In this study, we identified that a large fraction of adult thick-tufted rat layer 5 pyramidal neurons has an axon emanating from a basal dendrite (Fig. 1). These observations are in line with earlier reports using Golgi staining or EM from layer 2/3 or 5 pyramidal cells in a range of different cortical areas and species (19, 22, 23) or in hippocampal pyramidal neurons (20, 21) and support the notion that variation in axon location is a common principle of the cellular architecture of pyramidal cells. Cable theory predicts that the axial resistance between the AIS and the soma has a strong impact on spike initiation (11). Although the resistive coupling values across the population spanned more than one order of magnitude (from ~0.1 to 2.5 MΩ) (Fig. 3), we surprisingly could not identify a functional impact of AISΔ on somatically recorded AP properties (Table S3). To achieve uniform APs at the soma, our theoretical analyses and compartmental simulations predict that AISΔ should be inversely related with the local somatodendritic capacitance. The anatomical properties of layer 5 pyramidal neurons were well in line with these theoretical predictions and revealed a strong correlation, with the correct order of magnitude, with the apical dendrite diameter and number of dendritic nodes (Fig. 2 and Table S3). These experimental results support the theory of resistive coupling (11), predicting that the main determinants of the first component of the somatic AP are local geometry and intracellular resistivity.

Scaling of AIS location with somatodendritic morphology may be a general feature of neurons. For example, in midbrain dopaminergic neurons, axons often emanate from a dendrite that is larger in diameter (16–18). In these cells, the dendritic APs are electrically isolated during synaptic potentials and often characterized by temporal imprecision, failure, reverberation, and/or reflection (18). Because dopaminergic cells release neurotransmitter from somatodendritic sites, it is thought that dendritic origin of the AIS facilitates somatodendritic autoinhibition (18). In other cell types, the AIS location is linked to unique electrical computations. For example, in auditory neurons in chicks, the AIS distance, ranging between 0- and 50-μm distance, is adapted to enable frequency tuning (6, 13). Consistent with predictions from axial resistive coupling, the distal AIS position in these cells is characterized by smaller somatic AP amplitudes but with the distinct advantage of axonal AP output being phase-locked to higher input frequencies in the kilohertz range. Uncoupling the axon from charging the soma in some cell types, thus, benefits local axonal computations.

In pyramidal neurons, however, the AIS not only integrates incoming synaptic inputs and transforms them into output patterns but at the same time, plays a critical role in the antidromic direction to depolarize the somatodendritic membrane capacitance with sufficient magnitude and speed to activate the somatic Nav channels initiating the back-propagating spike (15, 29, 30). These observations of invariable somatic APs are in agreement with recordings in hippocampal CA1 pyramidal neurons with AIS distances ranging between ~1.0 and 20 μm showing little, if any, difference in the somatic AP (21). In that study, it was shown that axon coupling to basal dendrites facilitates synapse-evoked dendritic spike generation in the axon-carrying dendrite (21). Although we did not examine the presence of local basal dendritic spikes, our integrated electrophysiological and morphological approach suggests that the anatomical

arrangement may rather serve geometrical homeostasis, normalizing the amplitude and rise time of the somatic AP. Back-propagating APs are implicated in a wide range of dendritic computations (31), acting as a retrograde signal for nonlinear integrative functions in the dendritic branches of cortical pyramidal neurons (32–34). Tuning the position of the axon and local dendritic area may ensure amplitude and temporal fidelity of the back-propagating spike during its transition from the axon to the soma and dendritic branches.

The cellular and molecular mechanisms tuning the somatodendritic geometry together with the axon location remain to be determined. During the first weeks of development, when the dendritic tree rapidly expands, the AIS also shifts from its distal site to a more proximal location near the soma (35) and dynamically changes in length (36). One mechanism identified for activity-dependent changes in AIS location includes the Ca^{2+} influx from L-type Ca^{2+} channels subsequently activating the cytosolic signaling pathways, including the Ca^{2+}-calmodulin–sensitive phosphatase calcineurin (37). Such a molecular mechanism may also be suitable to link local somatodendritic Ca^{2+} elevations with cytoskeletal organization along the axon. This hypothesis remains to be established and would require simultaneous morphological analysis of dendrites and axons. The finding of a structural homeostatic scaling between axons and dendrites in pyramidal neurons may also have implications for the interpretation of activity-dependent relocation of the AIS along the longitudinal axis of the axon (5). Rather than reducing intrinsic excitability, our modeling predicts that shifting the AIS alone distally would weakly promote axonal firing (Fig. 5), consistent with theoretical and modeling results (9, 11). Furthermore, our results indicate that, in cortical pyramidal cells, the anatomical location of the AIS is to a large degree covarying with the local somatodendritic membrane area, ensuring the generation of uniform somatic APs in the face of highly variable dendritic loads.

Materials and Methods

All animal experiments were done in compliance with the European Communities Council Directive of November 24, 1986 (86/609/EEC) and were reviewed and approved by the animal welfare and ethics committee (DEC) of the KNAW under protocol number NIN 11.70. All details for electrophysiological recordings, numerical simulations, biophysical modeling, and compartmental NEURON modeling are described in *SI Materials and Methods*.

ACKNOWLEDGMENTS. We thank Koke Helmes for support in the acquisition of the initial data. This work was supported by the Ecole des Neurosciences de Paris (R.B.), Agence Nationale de la Recherche Grant ANR-14-CE13-0003 (to R.B.), an European Research Council (ERC) Starting Grant (European Union Seventh Framework Program Grant 261114), and National Multiple Sclerosis Society Grant RG 4924A1/1 (to M.H.P.K.).

1. Rasband MN (2010) The axon initial segment and the maintenance of neuronal polarity. *Nat Rev Neurosci* 11(8):552–562.
2. Kole MHP, Stuart GJ (2012) Signal processing in the axon initial segment. *Neuron* 73(2):235–247.
3. Xu K, Zhong G, Zhuang X (2013) Actin, spectrin, and associated proteins form a periodic cytoskeletal structure in axons. *Science* 339(6118):452–456.
4. King AN, Manning CF, Trimmer JS (2014) A unique ion channel clustering domain on the axon initial segment of mammalian neurons. *J Comp Neurol* 522(11):2594–2608.
5. Grubb MS, Burrone J (2010) Activity-dependent relocation of the axon initial segment fine-tunes neuronal excitability. *Nature* 465(7301):1070–1074.
6. Kuba H, Oichi Y, Ohmori H (2010) Presynaptic activity regulates Na(+) channel distribution at the axon initial segment. *Nature* 465(7301):1075–1078.
7. Kuba H, Yamada R, Ishiguro G, Adachi R (2015) Redistribution of Kv1 and Kv7 enhances neuronal excitability during structural axon initial segment plasticity. *Nat Commun* 6:8815.
8. Kaphzan H, Buffington SA, Jung JI, Rasband MN, Klann E (2011) Alterations in intrinsic membrane properties and the axon initial segment in a mouse model of Angelman syndrome. *J Neurosci* 31(48):17637–17648.
9. Gulledge AT, Bravo JJ (2016) Neuron morphology influences axon initial segment plasticity. *eNeuro* 3(1):ENEURO.0085-15.2016.
10. Baranauskas G, David Y, Fleidervish IA (2013) Spatial mismatch between the Na+ flux and spike initiation in axon initial segment. *Proc Natl Acad Sci USA* 110(10):4051–4056.
11. Brette R (2013) Sharpness of spike initiation in neurons explained by compartmentalization. *PLOS Comput Biol* 9(12):e1003338.
12. Eyal G, Mansvelder HD, de Kock CPJ, Segev I (2014) Dendrites impact the encoding capabilities of the axon. *J Neurosci* 34(24):8063–8071.
13. Kuba H, Ishii TM, Ohmori H (2006) Axonal site of spike initiation enhances auditory coincidence detection. *Nature* 444(7122):1069–1072.
14. Kole MHP, et al. (2008) Action potential generation requires a high sodium channel density in the axon initial segment. *Nat Neurosci* 11(2):178–186.
15. Stuart G, Spruston N, Sakmann B, Häusser M (1997) Action potential initiation and backpropagation in neurons of the mammalian CNS. *Trends Neurosci* 20(3):125–131.
16. Blythe SN, Wokosin D, Atherton JF, Bevan MD (2009) Cellular mechanisms underlying burst firing in substantia nigra dopamine neurons. *J Neurosci* 29(49):15531–15541.
17. Häusser M, Stuart G, Racca C, Sakmann B (1995) Axonal initiation and active dendritic propagation of action potentials in substantia nigra neurons. *Neuron* 15(3):637–647.
18. Gentet LJ, Williams SR (2007) Dopamine gates action potential backpropagation in midbrain dopaminergic neurons. *J Neurosci* 27(8):1892–1901.
19. Cajal SRY (1911) *Histologie du Système Nerveux de l'Homme & des Vertébrés* (A. Maloine, Paris).
20. Amaral DG (1978) A Golgi study of cell types in the hilar region of the hippocampus in the rat. *J Comp Neurol* 182(4 Pt 2):851–914.
21. Thome C, et al. (2014) Axon-carrying dendrites convey privileged synaptic input in hippocampal neurons. *Neuron* 83(6):1418–1430.
22. Palay SL, Sotelo C, Peters A, Orkand PM (1968) The axon hillock and the initial segment. *J Cell Biol* 38(1):193–201.
23. Peters A, Proskauer CC, Kaiserman-Abramof IR (1968) The small pyramidal neuron of the rat cerebral cortex. The axon hillock and initial segment. *J Cell Biol* 39(3):604–619.
24. Molnár Z, Cheung AFP (2006) Towards the classification of subpopulations of layer V pyramidal projection neurons. *Neurosci Res* 55(2):105–115.
25. Kim EJ, Juavinett AL, Kyubwa EM, Jacobs MW, Callaway EM (2015) Three types of cortical layer 5 neurons that differ in brain-wide connectivity and function. *Neuron* 88(6):1253–1267.
26. Groh A, et al. (2010) Cell-type specific properties of pyramidal neurons in neocortex underlying a layout that is modifiable depending on the cortical area. *Cereb Cortex* 20(4):826–836.
27. Rall W (1969) Time constants and electrotonic length of membrane cylinders and neurons. *Biophys J* 9(12):1483–1508.
28. Hamada MS, Kole MHP (2015) Myelin loss and axonal ion channel adaptations associated with gray matter neuronal hyperexcitability. *J Neurosci* 35(18):7272–7286.
29. Kole MHP, Stuart GJ (2008) Is action potential threshold lowest in the axon? *Nat Neurosci* 11(11):1253–1255.
30. Moore JW, Stockbridge N, Westerfield M (1983) On the site of impulse initiation in a neurone. *J Physiol* 336:301–311.
31. London M, Häusser M (2005) Dendritic computation. *Annu Rev Neurosci* 28:503–532.
32. Larkum M (2013) A cellular mechanism for cortical associations: An organizing principle for the cerebral cortex. *Trends Neurosci* 36(3):141–151.
33. Xu N-L, et al. (2012) Nonlinear dendritic integration of sensory and motor input during an active sensing task. *Nature* 492(7428):247–251.
34. Stuart G, Schiller J, Sakmann B (1997) Action potential initiation and propagation in rat neocortical pyramidal neurons. *J Physiol* 505(Pt 3):617–632.
35. Galiano MR, et al. (2012) A distal axonal cytoskeleton forms an intra-axonal boundary that controls axon initial segment assembly. *Cell* 149(5):1125–1139.
36. Gutzmann A, et al. (2014) A period of structural plasticity at the axon initial segment in developing visual cortex. *Front Neuroanat* 8:11.
37. Evans MD, et al. (2013) Calcineurin signaling mediates activity-dependent relocation of the axon initial segment. *J Neurosci* 33(16):6950–6963.
38. Bortone DS, Olsen SR, Scanziani M (2014) Translaminar inhibitory cells recruited by layer 6 corticothalamic neurons suppress visual cortex. *Neuron* 82(2):474–485.
39. Paxinos G, Watson C (2007) *The Rat Brain in Stereotaxic Coordinates* (Academic, Amsterdam), 6th Ed.
40. Hines ML, Carnevale NT (2001) NEURON: A tool for neuroscientists. *Neuroscientist* 7(2):123–135.
41. Schmidt-Hieber C, Bischofberger J (2010) Fast sodium channel gating supports localized and efficient axonal action potential initiation. *J Neurosci* 30(30):10233–10242.
42. Hallermann S, de Kock CPJ, Stuart GJ, Kole MHP (2012) State and location dependence of action potential metabolic cost in cortical pyramidal neurons. *Nat Neurosci* 15(7):1007–1014.
43. Battefeld A, Tran BT, Gavrilis J, Cooper EC, Kole MHP (2014) Heteromeric Kv7.2/7.3 channels differentially regulate action potential initiation and conduction in neocortical myelinated axons. *J Neurosci* 34(10):3719–3732.
44. Kole MHP, Bräuer AU, Stuart GJ (2007) Inherited cortical HCN1 channel loss amplifies dendritic calcium electrogenesis and burst firing in a rat absence epilepsy model. *J Physiol* 578(Pt 2):507–525.
45. Goodman DFM, Brette R (2009) The brian simulator. *Front Neurosci* 3(2):192–197.
46. Akers RM, Killackey HP (1978) Organization of corticocortical connections in the parietal cortex of the rat. *J Comp Neurol* 181(3):513–537.
47. Coombs JS, Curtis DR, Eccles JC (1957) The interpretation of spike potentials of motoneurones. *J Physiol* 139(2):198–231.
48. Kole MHP (2011) First node of Ranvier facilitates high-frequency burst encoding. *Neuron* 71(4):671–682.